

A wide-angle X-ray fibre diffraction method for quantifying collagen orientation across large tissue areas: application to the human eyeball coat

Jacek Klaudiusz Pijanka,^a Ahmed Abass,^b Thomas Sorensen,^c Ahmed Elsheikh^{b,d} and Craig Boote^{a*}

^aStructural Biophysics Group, School of Optometry and Vision Sciences, Cardiff University, Maindy Road, Cardiff CF24 4HQ, UK, ^bOcular Biomechanics Group, School of Engineering, University of Liverpool, Liverpool L69 3GH, UK, ^cDiamond Light Source Ltd, Didcot, Oxfordshire OX11 0DE, UK, and ^dNational Institute for Health Research (NIHR) Biomedical Research Centre, Moorfields Eye Hospital NHS Foundation Trust and UCL Institute of Ophthalmology, London, UK. Correspondence e-mail: bootec@cardiff.ac.uk

A quantitative map of collagen fibril orientation across the human eyeball coat, including both the cornea and the sclera, has been obtained using a combination of synchrotron wide-angle X-ray scattering (WAXS) and three-dimensional point mapping. A macromolecular crystallography beamline, in a custom-modified fibre diffraction setup, was used to record the 1.6 nm intermolecular equatorial reflection from fibrillar collagen at 0.5 mm spatial resolution across a flat-mounted human eyeball coat. Fibril orientation, derived as an average measure of the tissue thickness, was quantified by extraction of the azimuthal distribution of WAXS scatter intensity. Vector plots of preferential fibre orientation were remapped onto an idealized eyeball surface using a custom-built numerical algorithm, to obtain a three-dimensional representation of the collagen fibril architecture.

1. Introduction

The human eyeball coat is made up of the transparent cornea (forming approximately 15% of the ocular surface) and the white opaque sclera (~85%) (Bron *et al.*, 1997). Both tissues are continuous and together form a tough fibrous tunic that envelopes and protects the ocular contents. The cornea is responsible for about two-thirds of the total refractive power of the eye (Fatt & Weissman, 1992) and together with the sclera must be precisely shaped in order to cooperatively focus an image onto the retina. In addition, the sclera forms a protective supporting substrate for the vulnerable optic nerve axons as they exit the eye close to the posterior pole (Watson & Young, 2004).

The mechanical properties of the cornea and sclera are heavily influenced by their microstructure. A connective tissue stroma constitutes the bulk of the ocular coat and comprises a layered scaffold of collagen fibrils in an interfibrillar matrix of water, nonfibrous collagens, other proteins, proteoglycans and glycoproteins. Type I collagen is the most abundant molecule, with smaller quantities of types III and V. Collagen molecules form fibrils that are assembled into bundles and these, in turn, assemble into stacked lamellae (Maurice, 1957; Watson & Young, 2004). Fibrils within a lamella lie approximately parallel, with adjacent lamellae crossing at large angles throughout the tissue thickness. In the posterior cornea the lamellae are aligned approximately with the tissue surface, but

they are considerably more interwoven in the anterior cornea and in the sclera (Komai & Ushiki, 1991).

This complex fibrous network constitutes the eye's major load-bearing structure and, thus, its design is expected to reflect the mechanical stresses that the ocular tunic experiences both internally from the intraocular pressure and externally from forces applied to the eyeball, such as those exerted by the extraocular muscles. Since collagen fibrils are strongest axially, their preferential orientations dictate directions of maximal tissue stiffness (Hukins & Aspden, 1985; Boote *et al.*, 2005), and quantitative knowledge of collagen orientation will therefore be important in order to understand and model the mechanical behaviour of the eye and its compromise in surgery or disease. Indeed, modifications to the collagen orientation and/or associated tissue mechanics are closely linked with several common corneal and scleral pathologies (Meek *et al.*, 2005; McBrien *et al.*, 2009; Boote *et al.*, 2011; Pijanka *et al.*, 2012; Coudrillier, Tian *et al.*, 2012).

Experimental and numerical studies of the cornea and sclera in isolation have identified both tissues as nonlinear viscoelastic materials with significant anisotropy deriving from their preferential collagen alignment (Boote *et al.*, 2005; Pinsky *et al.*, 2005; Burgoyne *et al.*, 2005; Nguyen *et al.*, 2008; Elsheikh & Alhasso, 2009; Girard *et al.*, 2009; Elsheikh *et al.*, 2010; Lari *et al.*, 2012; Coudrillier, Boote *et al.*, 2012; Coudrillier, Tian *et al.*, 2012). However, corneal and scleral biomechanical behaviour is tightly coupled (Asejczyk-

Widlicka *et al.*, 2011), and accurate prediction of corneal, scleral and whole eye behaviour will therefore rely on detailed quantitative data on collagen orientation over the entire ocular coat.

Using a combination of split-line preparations and histology, Kokott (1938) was the first to attempt to qualitatively describe the bulk direction of collagen bundles over the eyeball coat. More recent studies to provide insight into corneal and scleral architecture have used imaging modalities such as transmission and scanning electron microscopy (Komai & Ushiki, 1991; Yamamoto *et al.*, 2000), atomic force microscopy (Yamamoto *et al.*, 1999) and second harmonic generation multiphoton microscopy (Han *et al.*, 2005; Winkler *et al.*, 2011). However, these techniques, whilst informative, have provided mainly localized and/or qualitative information. Over the past three decades, X-ray scattering methods have been used extensively to quantify collagen fibril orientation over the cornea (Daxer & Fratzl, 1997; Meek & Boote, 2009) and posterior scleral pole (Pijanka *et al.*, 2012) of the human eye. However, despite these efforts, approximately three-quarters of the human eyeball tunic awaits quantification. In the current study we addressed this shortfall by adapting a wide-angle X-ray scattering (WAXS) method that allows quantitative mapping of collagen fibril orientation across large tissue areas, and used this to examine whole flat-mounted human anterior and posterior eye cups. We also developed a numerical algorithm to remap the resulting two-dimensional data onto an idealized three-dimensional human eyeball surface.

2. Experiment

2.1. Tissue details and specimen preparation

All experimental procedures were performed in accordance with the Declaration of Helsinki. The complete left human eye globe of a 69-year-old male Caucasian donor with no history of ocular pathology or surgery was obtained within 24 h *post mortem* from the Fondazione Banca degli Occhi del Veneto, Italy. The external fat, muscle and episcleral tissues were

carefully removed and the optic nerve excised with a razor blade flush to the sclera. The globe was dissected approximately 2 mm behind the equator into two separate anterior and posterior cups, and the internal lens, retina and choroid tissues were removed. Eight relaxing incisions were made in the anterior cup from the specimen edge to the limbus (the ~1.5 mm-wide annular region of transition between the cornea and sclera), and four further incisions were made in the posterior cup from the specimen edge to the peripapillary sclera (the ~2 mm-wide annular region immediately surrounding the optic nerve) (Fig. 1). This dissection protocol prevented notable creasing of the corneal and scleral tissues upon subsequent flat mounting for X-ray measurement. The dissected cups were stored in 4% paraformaldehyde at 277 K until the time of X-ray exposure.

2.2. WAXS data collection

The uniformity in diameter and lateral spacing of collagen fibrils varies widely across the eyeball coat, these parameters being highly regular in the central cornea but much more polydisperse in the sclera (Meek, 2008). Since the equatorial collagen WAXS signal is derived from the molecular structure (Meek & Quantock, 2001), WAXS is more robust for following collagen organization across the whole corneo-scleral coat than is the case for small-angle X-ray scattering (SAXS), which derives from the fibrils themselves and has been adopted by other researchers to determine collagen orientation in the cornea (Daxer & Fratzl, 1997). Moreover, the collagen WAXS signal is less sensitive than SAXS to changes in tissue hydration, an advantage when moving between tissues of differing water content, such as the cornea and sclera (Meek & Boote, 2009).

WAXS experiments were carried out on macromolecular crystallography beamline I02 at the Diamond Light Source (Didcot, UK), in a custom fibre diffraction setup (Fig. 2). For data collection, the specimens were each separately wrapped in polyvinylidene chloride (PVC) film to prevent tissue dehydration, flattened by clamping between two rigid PVC

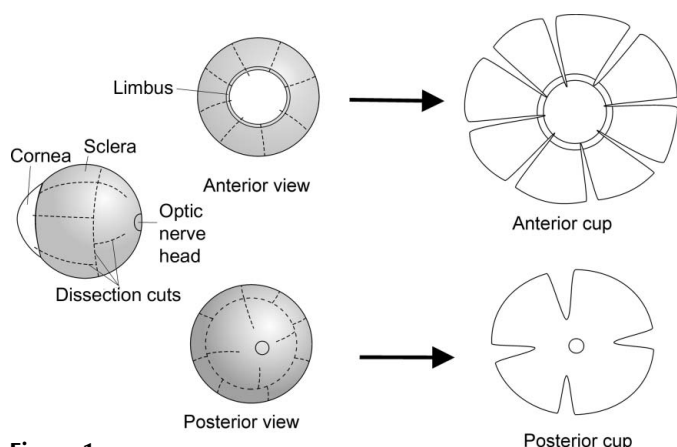


Figure 1
Dissection geometry used to enable flattening of the eyeball coat for WAXS experiments.

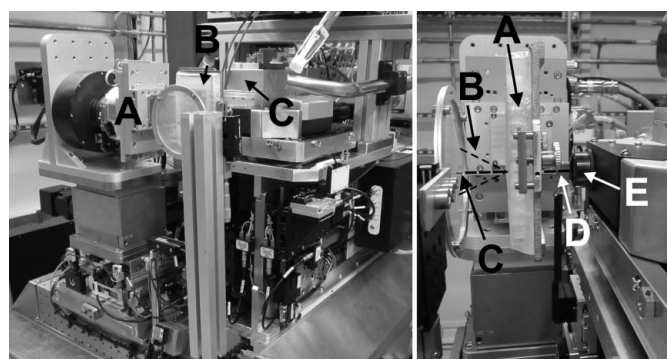


Figure 2
(Left panel) Station I02 at Diamond Light Source, modified for fibre diffraction experiments: A: goniometer; B: sample holder; C: MX beamline. (Right panel) Close-up of the specimen environment: A: sample holder; B: scattered X-ray path; C: beamstop; D: incident X-ray beam path; E: in-line VIS camera.

sheets, and mounted on a modified Perspex crystal well plate with a 50 mm-diameter central aperture to allow X-ray passage. The whole specimen assembly was then inserted into a metal well plate cartridge and mounted onto the beamline endstation using magnets, such that the incident X-ray beam was directed at the outer tissue surface and perpendicular to the plane of the flattened specimens. The beamline goniometer provided precise motorized horizontal and vertical specimen translation between X-ray exposures. WAXS patterns, each resulting from an X-ray exposure of 3 s, were collected at 0.5 mm horizontal/vertical intervals in a raster scan manner (Fig. 3), using a monochromatic focused X-ray beam of wavelength 0.09795 nm and cross-sectional diameter at the specimen measuring 0.2 mm. The patterns were recorded on an ADSC CCD detector placed 550 mm behind the specimen. A custom beamstop assembly, consisting of a 2 mm-diameter lead cylinder mounted in the centre of a Mylar sheet, prevented the unscattered beam from damaging the detector whilst allowing uninterrupted passage of the scattered X-rays.

2.3. WAXS data analysis

The WAXS pattern from the corneal and scleral stroma is dominated by a strong equatorial reflection originating from the regular lateral ~ 1.6 nm spacing of collagen molecules, aligned near axially within the stromal fibrils (Fig. 4) (Meek & Boote, 2009). Since every individual fibril within the stroma contributes scatter intensity to the WAXS pattern in a direc-

tion perpendicular to the molecular collagen axis, the distribution of X-ray scatter intensity as a function of the azimuthal angle provides a quantification of the distribution of molecular, and hence fibrillar, orientations within the tissue plane, as an average measure through the stromal depth (Meek & Boote, 2009; Pijanka *et al.*, 2012). Previous work has shown that the degree of collagen alignment varies with stromal depth, this being greatest in the deeper layers for the cornea (Abahussin *et al.*, 2009; Kamma-Lorger *et al.*, 2010) but, in contrast, being lowest in the deeper scleral layers near the posterior pole (Pijanka *et al.*, 2012). In the current study, depth-averaged data are presented across the whole cornea-scleral envelope.

The quantification of collagen fibril orientation from corneal and scleral WAXS patterns is described in detail elsewhere (Meek & Boote, 2009; Pijanka *et al.*, 2012). In brief, the radial intensity profile from each WAXS pattern was extracted to 256 equally spaced angular bins (each representing an azimuth sector of $\sim 1.4^\circ$) using a combination of image analysis (*Optimas 6.5*; Media Cybernetics Inc., Rockville, MD, USA) and spreadsheet (*Excel2003*; Microsoft Corporation, Redmond, WA, USA) software (Fig. 5). For each of the resulting 256 radial profiles, an individual power-law background function was fitted and subtracted from the intermolecular collagen scatter peak. This peak was then normalized for fluctuations in X-ray beam current and exposure time, and then radially integrated, resulting in a 1×256 matrix representing the angular distribution of total scatter intensity from fibrillar collagen. The distribution at this point could be divided into two components: isotropic scatter from collagen fibrils distributed equally in all directions in the plane of the tissue, and anisotropic scatter from fibrils preferentially oriented in one or more directions. Scattering from isotropic collagen was isolated and the anisotropic component was then plotted in polar vector coordinates using MATLAB software (The MathWorks Inc., Natick, MA, USA), with a 90° phase shift introduced because the recorded equatorial patterns are perpendicular to the fibril axis. Every sampled point in the specimen could thereby be represented as a polar vector plot, with the length of a vector in any direction indicating the relative number of fibrils preferentially oriented in that direction. In order to enable montage display of the data, the individual vector plots were scaled and normalized on the basis of their maximum value and a colour code assigned to express the magnitude of preferentially orientated collagen.

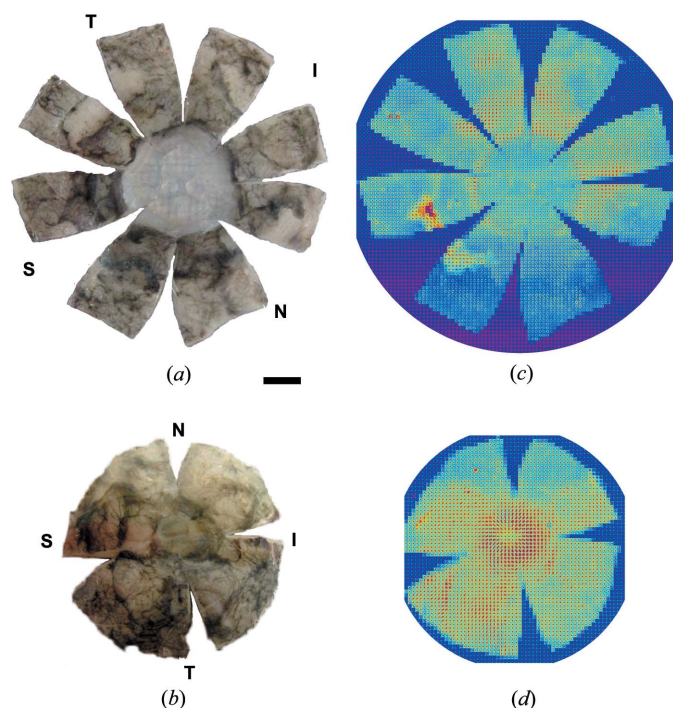


Figure 3
(a) Anterior and (b) posterior flat-mounted eyeball cups. (c), (d) Montages of individual WAXS patterns collected from (a) and (b), respectively. Bar: 5 mm. Letters S, I, N and T denote superior, inferior, nasal and temporal positions, respectively.

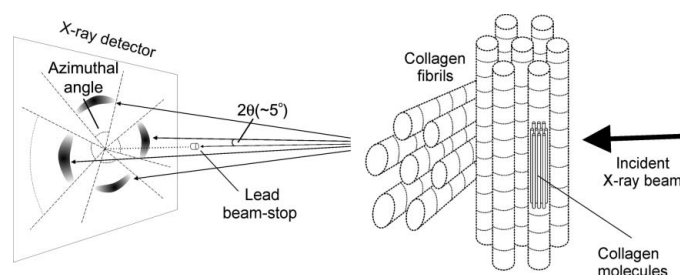


Figure 4
Schematic diagram showing the detection of an intermolecular equatorial WAXS pattern from fibrillar collagen.

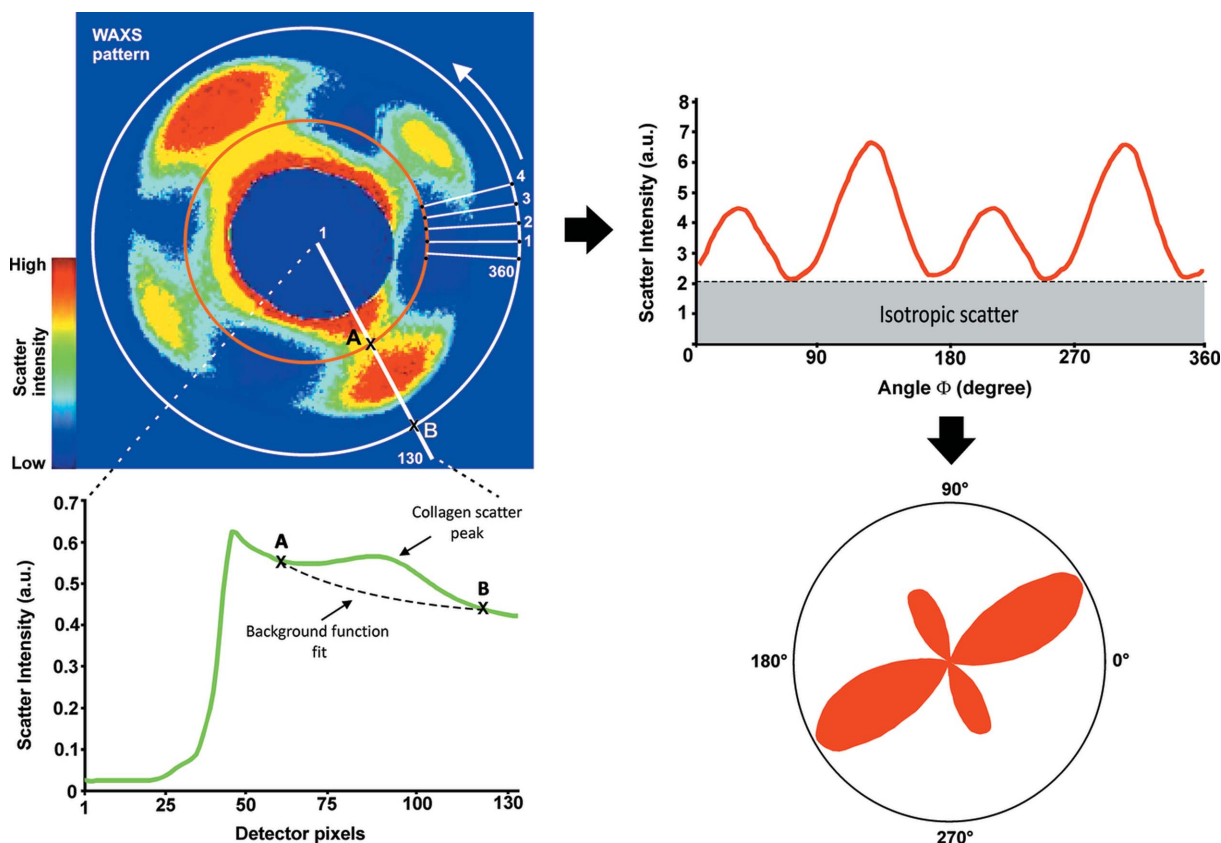


Figure 5 WAXS data processing. Following radial background fitting and subtraction, the azimuthal scatter intensity distribution is extracted. A polar vector plot of the anisotropic scatter component is then produced, in which the length of a vector in any direction is proportional to the number of collagen fibrils preferentially aligned in that direction.

All polar plots were subsequently assembled into a two-dimensional map of collagen preferential orientation across the specimen.

2.4. Two-dimensional to three-dimensional data remapping

A three-dimensional representation of the collagen fibril architecture was obtained by remapping the two-dimensional polar vector plots onto an idealized human eyeball surface template in MATLAB. Firstly, the geometric centre of the cornea was designated as the origin of the coordinate system, and eight reference lines were subsequently created, each representing an approximate centre line for one of the individual flattened tissue partitions of the anterior specimen (Fig. 6a). Every data point on the flattened specimens could then be located in two-dimensional space by a combination of its distances from the nearest centre line, $L2$, and from the origin, $L1$ (Figs. 6b and 6c). The located two-dimensional data points were then repositioned onto a three-dimensional human eyeball surface template. An idealized eye shape was constructed, which assumed that the cornea and sclera are spheres of radii 7.8 and 11.9 mm, respectively, and whose centres are separated by a distance 5.53 mm. The reference centre lines of the two-dimensional coordinate system were then projected onto the three-dimensional template for use as guidelines during the two-dimensional to three-dimensional

reshaping process (Fig. 7). The line closest to each two-dimensional data point was identified by calculating the smallest angle between each point and each of the eight centre lines, and then identifying the closest centre line to the point by minimizing the distance $L2$ (Fig. 6b). The side of the line on which a given point $P = [P(1), P(2)]$ lay was then detected by assuming that the reference line passed through the points $Q1 = [Q1(1), Q1(2)]$ and $Q2 = [Q2(1), Q2(2)]$ and using the equation

$$D = \text{sign}\{[Q2(1) - Q1(1)][P(2) - Q1(2)] - [Q2(2) - Q1(2)][P(1) - Q1(1)]\}, \quad (1)$$

where $D = -1$ for a two-dimensional point whose rotation lay in a clockwise direction from its corresponding reference line and $D = 1$ for a point lying counterclockwise. The distances $L1$ and $L2$ (Fig. 6b) were then detected for remapping onto the three-dimensional eyeball template (Fig. 8).

3. Results

A two-dimensional polar vector map of preferential collagen fibril orientation across the flat-mounted anterior human eyeball cup is presented in Fig. 9 and is shown remapped in three dimensions in Fig. 10. Equivalent data from the posterior specimen of the same eye are shown in Fig. 11.

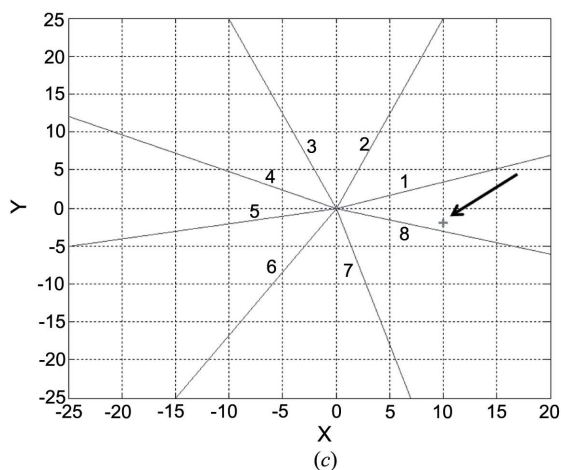
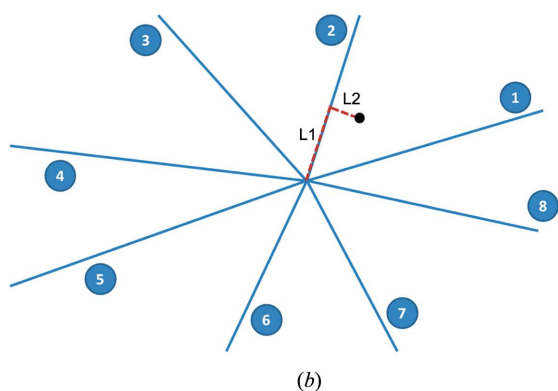
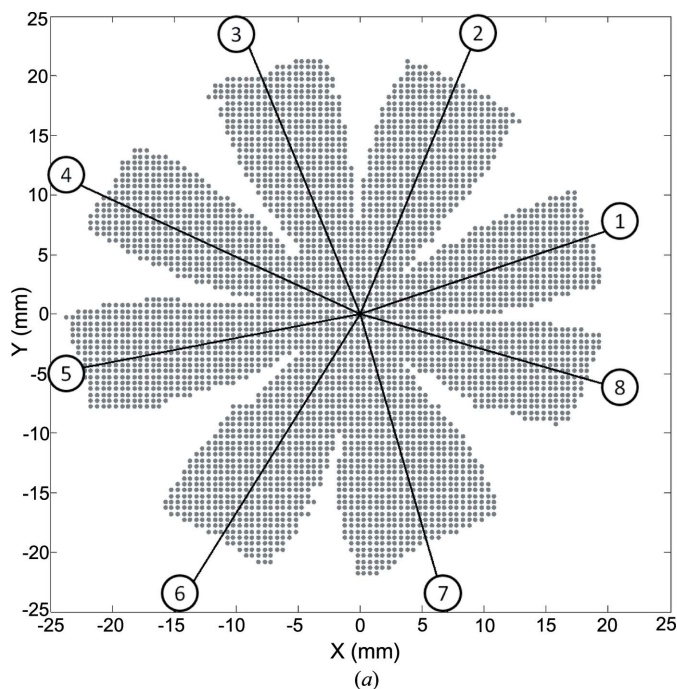


Figure 6 Referencing of the two-dimensional coordinate system. (a) The geometric centre of the cornea was chosen as the origin. Eight reference lines were created, each passing through the approximate mid-line of a segment of the dissected anterior specimen. (b) Two-dimensional point detection. A combination of the distance ($L2$) of each data point from its nearest reference line and its distance ($L1$) along the line from the origin is used as a reference. (c) Each data point is then referenced in the two-dimensional coordinate system.

Consistent with previous X-ray studies of the cornea (Daxer & Fratzl, 1997; Aghamohammadzadeh *et al.*, 2004; Boote *et al.*, 2005, 2006), an orthogonal preferential alignment of collagen along the superior–inferior and nasal–temporal corneal meridians is evident in the central cornea, gradually altering to a tangential orientation in the corneal periphery in order to merge with the predominantly circumferential fibrils of the limbus (Figs. 9 and 10).

In the anterior-most sclera, just behind the limbus, a complex pattern of preferential collagen alignment was revealed, with polar plots indicating spread of collagen fibril orientation in multiple directions (Figs. 9 and 10). Further back, at varying distances behind the limbus, four patches of highly aligned fibrils, running in a meridional direction, were noted (Fig. 9, broken lines). These patches correspond in location to the cardinal anatomical points of the eye globe – superior, inferior, nasal and temporal – and correlate with the insertion sites of the extraocular rectus muscles (Bron *et al.*, 1997). Collagen alignment between the meridional patches is evidently complex and spatially heterogeneous, in some areas

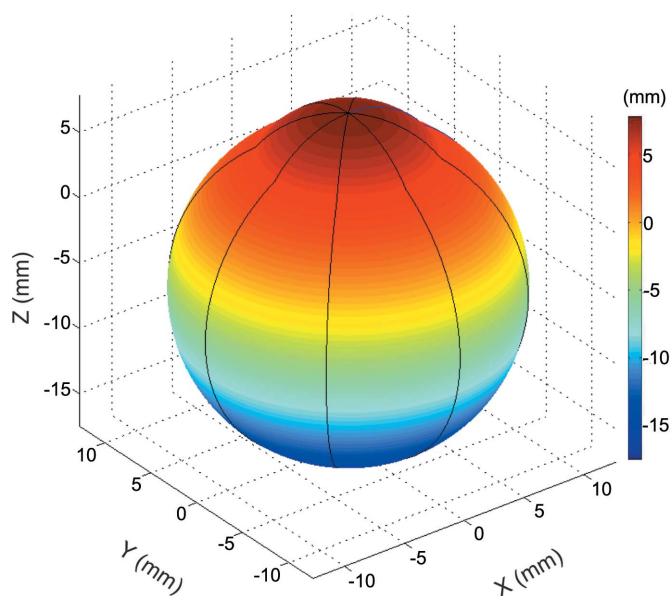


Figure 7 Three-dimensional surface template of an idealized human eye, with reshaped reference lines. The colour scale represents the distance along the Z axis.

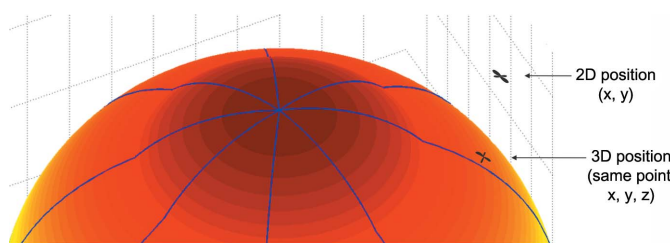


Figure 8 Remapping of a data point located in the two-dimensional coordinate system onto its corresponding location on the three-dimensional eyeball template.

preferential fibrils running parallel or slightly oblique to the equator, and in others running in multiple directions (Fig. 9). Along the equator, preferential fibril alignment in the sclera was mostly circumferential; however, notably in the inferior–nasal quadrant, this was replaced by largely meridional orientation (Fig. 9, arrow).

In the superior–temporal quadrant of the mid-posterior sclera, a large patch of highly aligned collagen fibrils, oriented in the inferior–temporal to superior–nasal direction, was observed (Fig. 11a, broken line), corresponding in location to the area between the oblique ocular muscle insertion sites (Bron *et al.*, 1997). The collagen orientation pattern in the remainder of the mid-posterior sclera was complex and regionally variable, but generally considerably less anisotropic, as reflected in the colour coding of the polar vector plots. The peripapillary sclera was characterized by a highly aligned circumferential ring of collagen surrounding the optic nerve head (Fig. 11a, broken annulus), consistent with previous WAXS studies of the posterior scleral pole (Pijanka *et al.*, 2012). The above novel scleral features were verified in a

second left eye from a male normal human donor, also aged 69 years (Figs. 9 and 11a, insets).

The current study also revealed that a considerable proportion of the corneal and scleral collagen throughout the stromal thickness is arranged in an isotropic manner. This component may also be expected to contribute significantly to the biomechanical properties of the tissue. Figs. 12(a) and 12(b) show contour maps of the distribution of isotropic fibrillar collagen across the anterior and posterior specimens, respectively. Notable variations in isotropic collagen content occur with anatomical position across the eyeball coat, and are particularly marked in the scleral regions near the muscle insertion and optic nerve entry sites.

4. Discussion

In this paper we present a synchrotron WAXS method for quantifying bulk collagen alignment over large tissue areas, which has been used to obtain a quantitative map of collagen fibril orientation across the human eyeball coat. The current

work extends our previous WAXS studies of the ocular envelope, which have until now been restricted to the cornea (Meek & Boote, 2009) and posterior scleral pole (Pijanka *et al.*, 2012). As such, the method presented here will improve current modelling of ocular biomechanics by providing detailed numerical data on collagen architecture in the intervening scleral tissue, which constitutes around 75% of the eyeball surface and has, thus far, not been quantified. This will complement future experimental efforts aimed at characterizing ocular mechanical performance, which are also expected to focus on whole eye globe testing on account of its superior reliability to methods that test the cornea and sclera in isolation.

The findings presented herein support existing reports of collagen anisotropy in the anterior (Meek & Boote, 2009) and posterior (Pijanka *et al.*, 2012) poles of the human eye, all of which have been linked with mechanical function. Specifically, inferior–superior and temporal–nasal preferential collagen orientation in the central cornea is possibly designed to resist the pulling forces of the extra-ocular recti muscles during eye movement and image fixation (Daxer & Fratzl, 1997; Boote *et al.*, 2005), while circumferential collagen at the limbus may be required to withstand the increased stress brought about by the

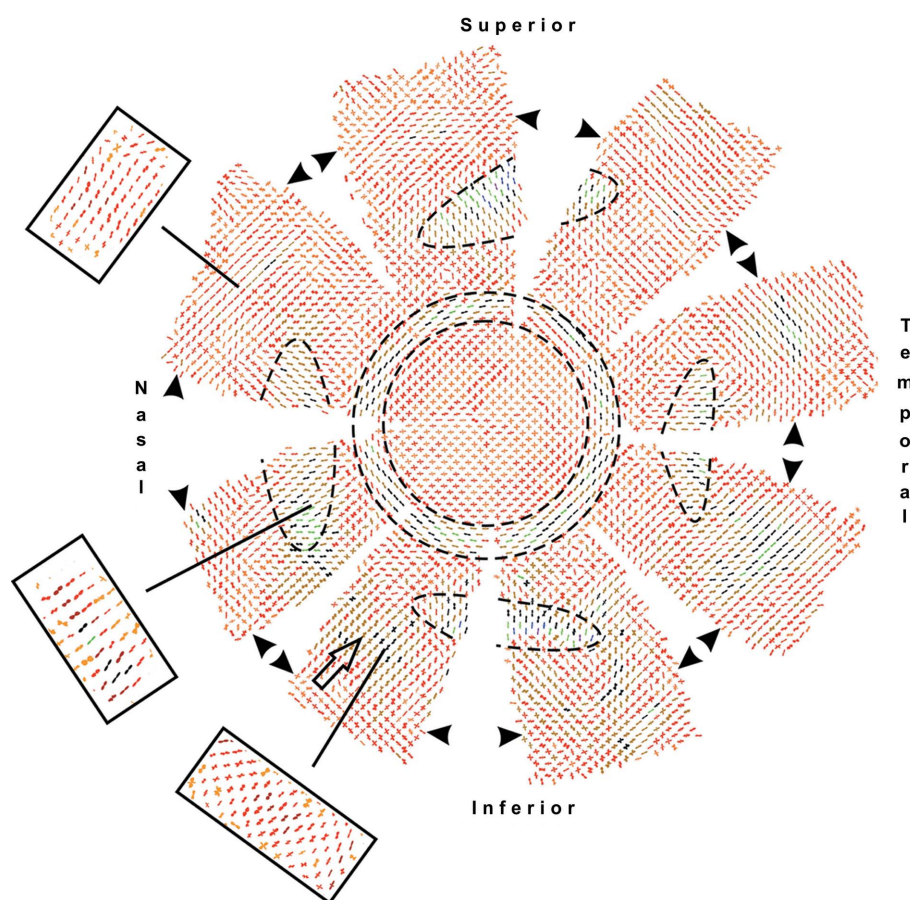


Figure 9
Two-dimensional map of polar vector plots showing preferential orientation of collagen fibrils at 0.5 mm intervals over the flattened anterior specimen. (Broken annulus) Circumferential alignment of collagen is evident in the limbus. (Broken lines) Meridional fibril alignment at cardinal points in the anterior sclera, corresponding to rectus muscle insertion sites. (Arrow heads) Geometric equator of the eye globe. (Arrow) Localized meridional collagen alignment in equatorial sclera. Insets: equivalent data from a second eye, confirming the presence of highlighted features. Colour coding for vector plot scaling: orange (×1), red (×2), brown (×3), black (×4), green (×5), blue (×6), purple (×7).

change in tissue curvature at the corneo-scleral border (Maurice, 1988; Boote *et al.*, 2009). At the posterior pole, the existence of a collagen annulus in the peripapillary sclera (Pijanka *et al.*, 2012) is structurally optimal for preventing excessive scleral canal expansion under elevated intraocular pressure and hence may provide a neuroprotective function for the optic nerve axons (Grytz *et al.*, 2011).

In addition, the current data have characterized further anisotropic features of the sclera that are consistent with a mechanical adaption of the tissue. Four regions of highly aligned meridional fibrils were noted at the cardinal points of the anterior tissue, slightly forward of the equator. These features were also noted in qualitative studies (Kokott, 1938) and probably serve to transfer tension from the extraocular recti muscles to the eyeball coat in facilitating eye movements. Similarly, we further contend that the patch of highly aligned

collagen fibrils, oriented inferior–temporal to superior–nasal, and located in the superior–temporal mid-posterior sclera, is required locally to mechanically reinforce the tissue along the directions of force exerted by the superior and inferior oblique muscles.

Whilst the equatorial sclera exhibited comparatively less structural anisotropy than the anterior and posterior tissue, a general preference for circumferential alignment was discernible, with a significant departure in the inferior–nasal quadrant where meridionally oriented fibrils dominated. These observations are also in general agreement with the early work of Kokott (1938). Mechanically, a predominantly

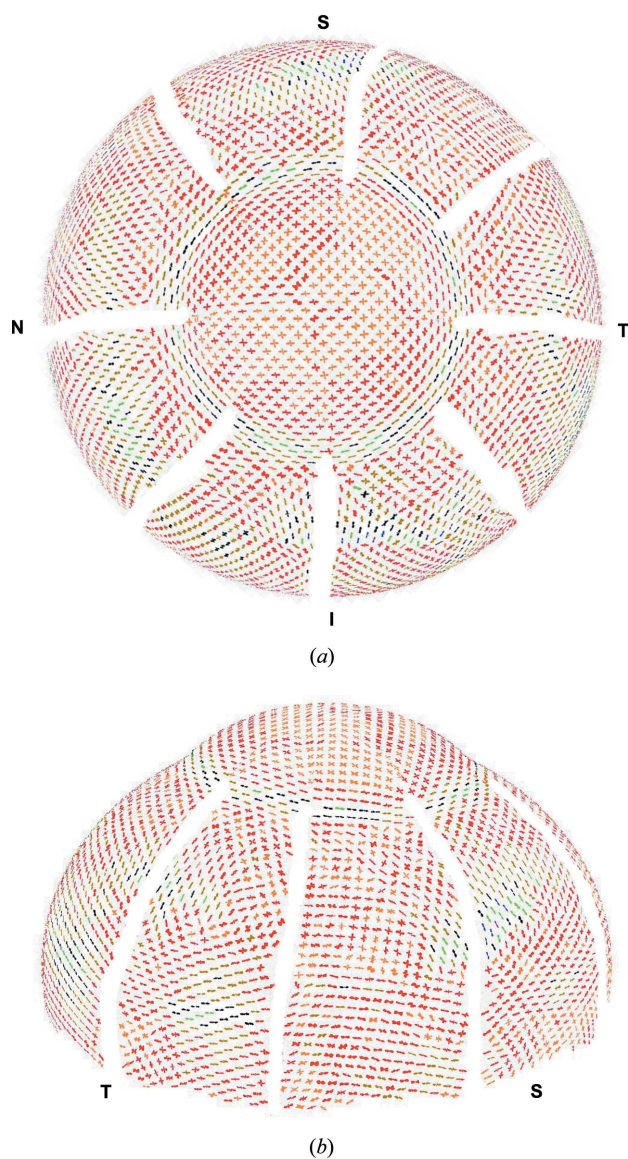


Figure 10 Three-dimensional surface representation of the anterior collagen polar vector map. (a) Plan view. S, I, N and T denote superior, inferior, nasal and temporal positions, respectively. (b) Angled view.

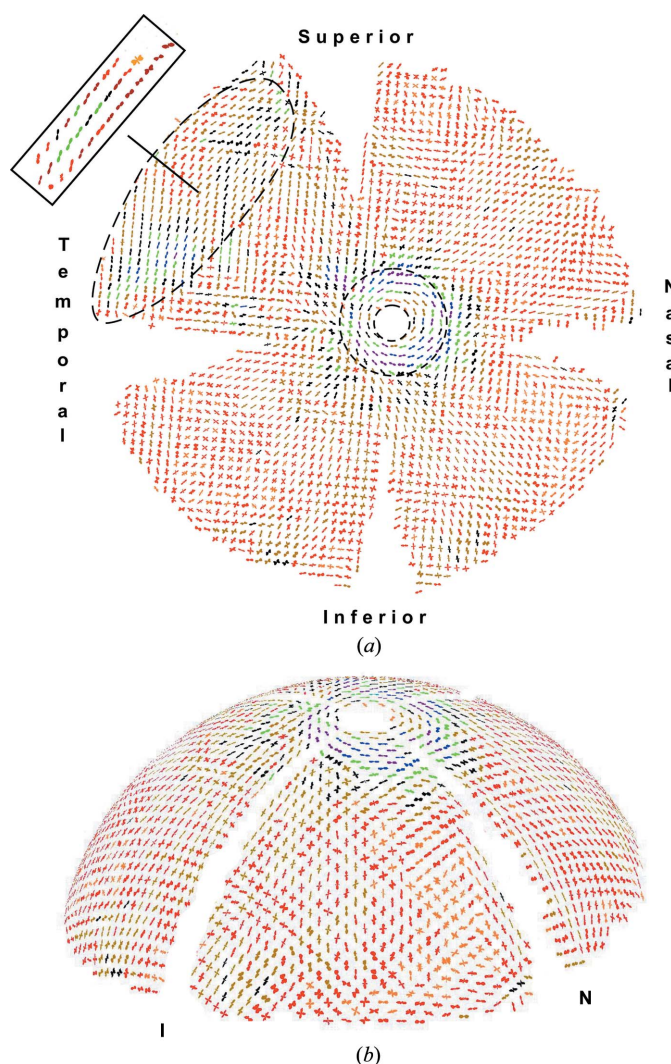


Figure 11 (a) Two-dimensional map of polar vector plots showing preferential orientation of collagen fibrils at 0.5 mm intervals over the flattened posterior specimen. (Broken annulus) Circumferential alignment of collagen around the optic nerve head is evident in the peripapillary sclera. (Broken line) Strong uniaxial alignment evident in the superior–temporal mid-posterior sclera, corresponding to oblique muscle insertion sites. Inset: equivalent data from a second eye, confirming the presence of highlighted features. Colour coding for vector plot scaling: orange ($\times 1$), red ($\times 2$), brown ($\times 3$), black ($\times 4$), green ($\times 5$), blue ($\times 6$), purple ($\times 7$), turquoise ($\times 10$). (b) Three-dimensional surface representation of the posterior collagen polar vector map. I and N denote inferior and nasal positions.

circumferential arrangement of fibrils at this location may prevent equatorial bulging of the scleral shell under intraocular pressure (Girard *et al.*, 2009). In contrast to our measurements in the human eye, previous analysis of the rat sclera using light scattering reported largely meridional fibres at the equator. These features were said to be too extensive to be accounted for by the presence of nearby rectus muscle insertions alone, and it was proposed that they may exist partly to minimize axial elongation of the eyeball (Girard *et al.*, 2011). Such a scheme appears inconsistent with the current human data, in which clear meridional orientation was only observed in a localized region of the inferior–nasal equatorial sclera. Differences in scleral collagen organization between rat and human sclera may reflect the differing overall shape of the eye globe in rats and humans and the mode of eye movements

and image fixation. Since these properties appear to affect the architecture of corneal collagen, resulting in differences between mammalian species (Hayes *et al.*, 2007), we speculate that they may also partly dictate the organization of scleral collagen.

This study was subject to a number of experimental limitations. Firstly, dissecting and flattening of the eyeball coat may be expected to release some of the residual stress present within the intact tissue, potentially leading to changes in the natural orientation of collagen, particularly near the cut edges. However, studies in other collagenous tissues suggest that this effect is more predominant at the macro (organ) level and less so at the level of the collagen microstructure (Lanir, 2009). Moreover, fixing the eyeball coat in its natural curvature will probably have further minimized any collagen reorganization. Nevertheless, the data points immediately adjacent to cuts were ignored in our interpretation. Secondly, variations in tissue hydration over the eyeball coat may have impacted on the overall intensity of the collagen scatter, affecting the relative scaling (but not the shape) of the individual vector plots. However, as mentioned, this effect is likely to be minimal when measuring the intermolecular signal (Meek & Boote, 2009). Furthermore, use of paraformaldehyde fixation may have helped to normalize any hydration variations across the tissue. Thirdly, the model used for remapping the two-dimensional data onto the three-dimensional eyeball surface was based on an average human eyeball size of idealized shape. These approximations led to some gaps and overlaps of data in the resulting three-dimensional renderings. While overlapping data points were removed for clarity, gaps arising from model inaccuracy are still evident in the resulting three-dimensional figures. In the future, specimen-specific eye dimensions will be obtained for mapping of WAXS data onto individual eyeball shapes, using intact globe inflation/imaging methods currently under development in our laboratory.

5. Conclusion

The current study demonstrates that obtaining detailed quantitative information on collagen architecture from the whole eyeball surface without excessive sample preparation is feasible using WAXS. The results obtained support the growing idea that the collagen architecture of the ocular coat is mechanically adapted for visual function. Although this concept is not new, novel quantitative data of the kind presented herein will benefit future numerical simulation of whole eye mechanical behaviour, potentially leading to improved understanding of the role of altered ocular structure and biomechanics in pathologies such as glaucoma and myopia, as well as better prediction of the eye’s response to surgical and therapeutic intervention.

This work was supported by Fight For Sight Project grant 1360 (to CB), Science and Technology Facilities Council beamtime award MX7062 (to CB and AE), and the National Institute for Health Research (NIHR) Biomedical Research

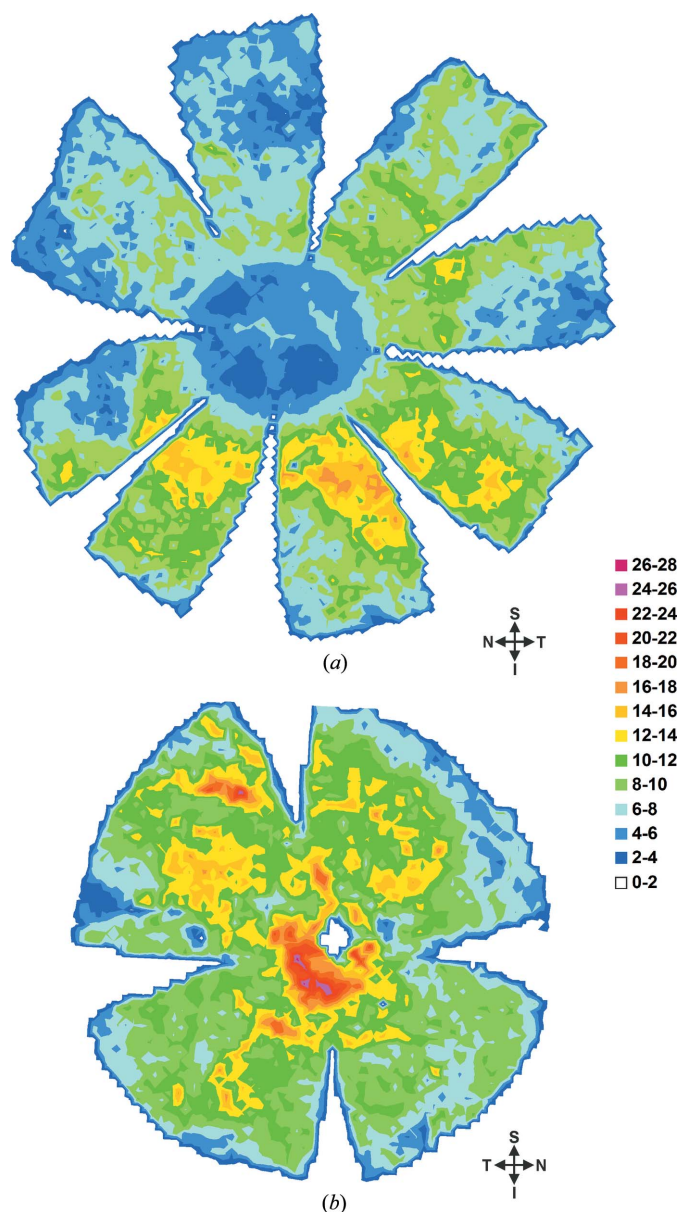


Figure 12 Contour map of isotropic collagen scatter (arbitrary units). (a) Anterior and (b) posterior specimens.

Centre based at Moorfields Eye Hospital NHS Foundation Trust and UCL Institute of Ophthalmology (AE). The views expressed are those of the author(s) and not necessarily those of the NHS, the NIHR or the Department of Health of the United Kingdom. The authors thank Mr Matthew Dunn for useful discussion.

References

- Abahussin, M., Hayes, S., Knox Cartwright, N., Kamma-Lorger, C., Khan, Y., Marshall, J. & Meek, K. (2009). *Invest. Ophthalmol. Vis. Sci.* **50**, 5159–5164.
- Aghamohammadzadeh, H., Newton, R. H. & Meek, K. M. (2004). *Structure*, **12**, 249–256.
- Asejczyk-Widlicka, M., Śródka, W., Schachar, R. A. & Pierścioneck, B. K. (2011). *J. Biomech.* **44**, 543–546.
- Boote, C., Dennis, S., Huang, Y., Quantock, A. J. & Meek, K. M. (2005). *J. Struct. Biol.* **149**, 1–6.
- Boote, C., Elsheikh, A., Kassem, W., Kamma-Lorger, C. S., Hocking, P. M., White, N., Inglehearn, C. F., Ali, M. & Meek, K. M. (2011). *Invest. Ophthalmol. Vis. Sci.* **52**, 1243–1251.
- Boote, C., Hayes, S., Abahussin, M. & Meek, K. (2006). *Invest. Ophthalmol. Vis. Sci.* **47**, 901–908.
- Boote, C., Hayes, S., Young, R. D., Kamma-Lorger, C. S., Hocking, P. M., Elsheikh, A., Inglehearn, C. F., Ali, M. & Meek, K. M. (2009). *J. Struct. Biol.* **166**, 195–204.
- Bron, A. J., Tripathi, A. C. & Tripathi, B. J. (1997). *The Cornea and Sclera*, 8th ed. London: Chapman and Hall.
- Burgoyne, C. F., Downs, J. C., Bellezza, A. J., Suh, J. K. F. & Hart, R. T. (2005). *Prog. Retin. Eye Res.* **24**, 39–73.
- Coudrillier, B., Boote, C., Quigley, H. A. & Nguyen, T. D. (2012). *Biomech. Model Mechanobiol.* doi:10.1007/s10237-012-0455-y.
- Coudrillier, B., Tian, J., Alexander, S., Myers, K. M., Quigley, H. A. & Nguyen, T. D. (2012). *Invest. Ophthalmol. Vis. Sci.* **53**, 1714–1728.
- Daxer, A. & Fratzl, P. (1997). *Invest. Ophthalmol. Vis. Sci.* **38**, 121–129.
- Elsheikh, A. & Alhasso, D. (2009). *Exp. Eye Res.* **88**, 1084–1091.
- Elsheikh, A., Geraghty, B., Alhasso, D., Knappett, J., Campanelli, M. & Rama, P. (2010). *Exp. Eye Res.* **90**, 624–633.
- Fatt, I. & Weissman, B. (1992). *Physiology of the Eye: An Introduction to the Vegetative Functions*, 2nd ed. Boston: Butterworth-Heinemann.
- Girard, M. J., Dahlmann-Noor, A., Rayapureddi, S., Bechara, J. A., Bertin, B. M., Jones, H., Albon, J., Khaw, P. T. & Ethier, C. R. (2011). *Invest. Ophthalmol. Vis. Sci.* **52**, 9684–9693.
- Girard, M. J., Downs, J. C., Burgoyne, C. F. & Suh, J. K. (2009). *J. Biomech. Eng.* **131**, 051011.
- Grytz, R., Meschke, G. & Jonas, J. B. (2011). *Biomech. Model Mechanobiol.* **10**, 371–382.
- Han, M., Giese, G. & Bille, J. F. (2005). *Opt. Express*, **13**, 5791–5797.
- Hayes, S., Boote, C., Lewis, J., Sheppard, J., Abahussin, M., Quantock, A. J., Purslow, C., Votruba, M. & Meek, K. M. (2007). *Anat. Rec. Adv. Integr. Anat. Evol. Biol.* **290**, 1542–1550.
- Hukins, D. W. L. & Aspden, R. M. (1985). *Trends Biochem. Sci.* **10**, 260–264.
- Kamma-Lorger, C., Boote, C., Hayes, S., Moger, J., Burghammer, M., Knupp, C., Quantock, A., Sorensen, T., Di Cola, E., White, N., Young, R. & Meek, K. (2010). *J. Struct. Biol.* **169**, 424–430.
- Kokott, W. (1938). *Arch. Ophthalmol.* **138**, 424–485.
- Komai, Y. & Ushiki, T. (1991). *Invest. Ophthalmol. Vis. Sci.* **32**, 2244–2258.
- Lanir, Y. (2009). *J. Biomech. Eng.* **131**, 044506.
- Lari, D. R., Schultz, D. S., Wang, A. S., Lee, O. T. & Stewart, J. M. (2012). *Exp. Eye Res.* **94**, 128–135.
- Maurice, D. M. (1957). *J. Physiol.* **136**, 263–286.
- Maurice, D. M. (1988). *The Cornea: Transactions of the World Congress on the Cornea III*, edited by H. D. Cavanagh, pp. 187–192. New York: Raven Press.
- McBrien, N. A., Jobling, A. I. & Gentle, A. (2009). *Optom. Vis. Sci.* **86**, E23–E30.
- Meek, K. M. (2008). *Collagen: Structure and Mechanics*, edited by P. Fratzl, pp. 359–396. New York: Springer.
- Meek, K. M. & Boote, C. (2009). *Prog. Retin. Eye Res.* **28**, 369–392.
- Meek, K. M. & Quantock, A. J. (2001). *Prog. Retin. Eye Res.* **20**, 95–137.
- Meek, K. M., Tuft, S. J., Huang, Y. F., Gill, P. S., Hayes, S., Newton, R. H. & Bron, A. J. (2005). *Invest. Ophthalmol. Vis. Sci.* **46**, 1948–1956.
- Nguyen, T. D., Jones, R. E. & Boyce, B. L. (2008). *J. Biomech. Eng.* **130**, 041020.
- Pijanka, J. K., Coudrillier, B., Ziegler, K., Sorensen, T., Meek, K. M., Nguyen, T. D., Quigley, H. A. & Boote, C. (2012). *Invest. Ophthalmol. Vis. Sci.* **53**, 5258–5270.
- Pinsky, P. M., Van der Heide, D. & Chernyak, D. (2005). *J. Cataract. Refract. Surg.* **31**, 136–145.
- Watson, P. G. & Young, R. D. (2004). *Exp. Eye Res.* **78**, 609–623.
- Winkler, M., Chai, D., Kriling, S., Nien, C. J., Brown, D. J., Jester, B., Juhasz, T. & Jester, J. V. (2011). *Invest. Ophthalmol. Vis. Sci.* **52**, 8818–8827.
- Yamamoto, S., Hashizume, H., Hitomi, J., Shigeno, M., Sawaguchi, S., Abe, H. & Ushiki, T. (2000). *Arch. Histol. Cytol.* **63**, 127–135.
- Yamamoto, S., Hitomi, J., Sawaguchi, S., Abe, H., Shigeno, M. & Ushiki, T. (1999). *Nippon Ganka Gakkai Zasshi*, **103**, 800–805.